Strength-limiting damage and its mitigation in CAD-CAM zirconia-reinforced lithium-silicate ceramics machined in a fully crystallized state

Dan L Romanyk, Yilan Guo, Nyssa Rae, Sydney Veldhuis, Slobodan Sirovica, Garry JP Fleming, Owen Addison

Objectives: The objective was to explore how clinically relevant machining process and heat treatment influence damage accumulation and strength degradation in lithium silicate-based glass ceramics machined in the fully crystallized state.

Methods: A commercial zirconia-reinforced lithium silicate (ZLS) glass ceramic with a fully developed microstructure (Celtra® Duo) was studied. Disk-shaped specimens (nominal 10 mm diameter and 1 mm thickness) were fabricated either using a CAD-CAM process, creating a clinically relevant dental restoration surface, or were sectioned from water-jet cut cylindrical blocks with their critical surfaces consistently polished. Bi-axial flexure strength (BFS) was determined in a ball-on-ring configuration, and fractographic analysis was performed on failed specimens. XRD, AFM and SEM measurements were conducted before and after heat treatment. For each sample group, BFS was correlated with surface roughness. A two-way ANOVA and post-hoc Tukey tests were used to determine differences in BFS between machining and heat treatment groups ($\alpha=0.05$).

Results: A two-way ANOVA demonstrated that BFS was influenced by fabrication route ($p<0.01$) with CAD-CAM specimens exhibiting significantly lower mean BFS. A factorial interaction was observed between heat treatment and machining route ($p<0.01$), where a significant strengthening effect of post-manufacture heat treatment was noted for CAD-CAM specimens but not sectioned and polished samples. CAD-CAM specimens exhibited sub-surface lateral cracks alongside radial cracks near fracture origin which were not observed for polished specimens. BFS did not correlate with surface roughness for polished specimens, and no change in microstructure was detectable by XRD following heat treatment.

Significance: The mechanical properties of the ZLS ceramic material studied were highly sensitive to the initial surface defect integral associated with manufacturing route and order of operations. CAD-CAM manufacturing procedures result in significant strength-limiting damage which is likely to influence restoration performance; however, this can be partially mitigated by post-machining heat treatment.

1. Introduction

Developments in intra-oral three-dimensional (3D) imaging and 'chair-side' computer aided design – computer aided manufacturing (CAD-CAM) have resulted in efficient dental digital workflows for prosthesis fabrication, which reduce patient treatment times compared with traditional methodologies. However, a rate-limiting step for the manufacturing of all-ceramic restorations is the necessity to perform post-machining treatments to improve the mechanical properties including toughness and flexural strength prior to clinical use [1]. Machining of the ceramic substrate in a precursor form - which lacks the final microstructure, is typically required to balance machining efficiency and machining tool longevity with the accumulation of strength-limiting damage in the machined prosthesis [2-4]. Heat treatments are subsequently used to develop the microstructure by sintering of zirconia ceramics and crystallization of lithium silicate glass-ceramics. However, heat treatments are often undesirable, increasing patient treatment times between tooth preparation and restoration placement. As a consequence, material developments have been targeted at eliminating or reducing lengthy post-machining heat treatments processes.

Currently, the most common substrates used for the 'chair-side' manufacture of all-ceramic restorations are lithium silicate based glass-ceramics, which can accurately mimic the shade, translucency and lustre of the natural dentition [5]. Much of the evidence demonstrating the long-term clinical success of CAD-CAM lithium silicate glass-ceramics has been generated for one commercial material, namely, IPS e.max® CAD (Ivoclar Vivadent Inc) [6,7]. IPS e.max® CAD contains a lithium metasilicate crystalline phase and requires a post-machining heat treatment to crystallise the lithium disilicate which largely replaces the lithium metasilicate [8]. A recent development of lithium silicate glass-ceramics is the incorporation of zirconia dissolved in the parent glass. The zirconia is not present in a crystalline form, but rather acts alongside phosphorus pentoxide as a nucleating agent and results in a final ceramic microstructure comprised of lithium metasilicate crystals surrounded by nanometric lithium orthophosphate crystals and a minor lithium disilicate crystalline fraction within the residual glass [9-12]. Zirconia-reinforced lithium silicate (ZLS) glass-ceramics are advocated to be machined in either a

partially crystallized form (Vita Suprinity®, Vita Zahnfabrik) or alternatively with a 'fully developed' microstructure (Celtra® Duo, Dentsply Sirona). The manufacturer of Celtra® Duo advocates that considerable clinical efficiencies can be gained by machining ZLS with a 'fully developed' microstructure [13], such that dental prostheses can be milled and manually polished prior to insertion in as little as ~15 mins, or with the addition of a glazing firing cycle - which reportedly acts to strengthen the ceramic, in ~30 mins [13].

The multipoint contact grinding processes used in dentistry to shape the prosthesis in chair-side CAD-CAM are known to introduce complex patterns of surface and subsurface damage which limit the strength of the prosthesis [1-4,12]. Material removal during machining occurs when diamond particles embedded in the surfaces of rotating burs contact the ceramic thereby generating high surface strains which initiate microcracking and chip fragment formation [15-17]. The contact between the abrasive and the surface also results in residual cracks, both normal to and parallel with the cut surface, which interact with a subsurface residual stress field created through both plastic deformation and heat generated by friction [15-18]. Machining damage has been shown to extend to at least 50 μm from the surface and is microstructure dependent, with the hardness and toughness of the substrate determining the magnitude of the machining contact forces [1,19]. Therefore, the resultant surface defect population and the residual stresses dictate the effective strength of the restoration, but both may be modified by post-machining heat treatments [20].

The primary aim of the study was to determine the impact of surface damage generated by a clinically relevant CAD-CAM process on the strength of a ZLS glass-ceramic machined in a fully crystallized form and to relate the findings to the nature of surface damage accumulation during machining. The secondary aim was to assess how the order of post-machining procedures that result in a modification of surface defects and residual stress states, including heat treatment, influence the mitigation of machining associated surface damage.

2. Materials and Methods

2.1 CAD-CAM test specimen preparation

A zirconia reinforced (10 wt% zirconium dioxide) lithium silicate ceramic, Celtra® Duo HT (Lot# 18028463, Dentsply Sirona, USA) was acquired in the form of prefabricated blocks (12 × 14 × 18 mm) for use in a 'chair-side' dental CAD-CAM unit. Two groups of nominally identical disk-shaped specimens (n=15) were fabricated using a CAD-CAM workflow. In accordance with a previous study, 10 mm diameter and 1.0 ± 0.1 mm thickness disk-shaped specimens were machined using a Sirona CEREC MC X 'chair-side' milling unit (Dentsply Sirona, USA) from the prefabricated blocks [1]. A CAD template was acquired by scanning an equivalent geometry disk-shaped mould with a CEREC Omnicam (Dentsply Sirona, USA) and the design was completed in CEREC v4.5 software. New bur sets were installed before the machining of each disk-group investigated, and each disk was labelled on the upper surface following machining to ensure a consistent orientation for both subsequent heat treatment and mechanical testing protocols. The tab left by machining (close to the upper surface) was manually removed using SiC abrasive paper under water lubrication prior to mechanical testing. One group of CAD-CAM specimens received no further processing (CAD) while the second group were heat treated (CAD-HT). The heat treated specimens were orientated with the marked upper surfaces not in contact with the firing slab and subjected to the manufacturer's recommended 'polish and fire' cycle in an Ivoclar Vivadent Programat EP 5000 furnace. The 'polish and fire' cycle involved the disk-shaped specimens being pre-heated at 500°C for 2 mins, the temperature increased at 60°C/min to 820°C, held for 1 min prior to long term cooling from 750°C.

2.2 Control surface test specimen preparation

Four additional groups of specimens (n=15) were fabricated by first reducing the rectangular prefabricated Celtra® Duo blocks to 10 mm diameter cylinders (nominal) using water-jet cutting. Disks of 10 mm diameter and 1.0 ± 0.1 mm thickness were subsequently sectioned from the prepared cylinders using a diamond blade in an IsoMet 5000 precision saw (Buehler, USA) at a blade speed of 300 rpm and a feed rate of 4.0 mm/min, using water coolant. One group of disk-shaped specimens received no

further treatment (CUT). In the second group, specimens were manually polished on one surface sequentially using SiC abrasive papers (P800, P1000, P1500 and P2000 grits) for fixed time intervals of 90 s using water as a lubricant (POL). A further group of disk-shaped specimens were manually polished in accordance with procedure above (POL) and then heat-treated according to 'polish and fire' cycle previously outlined (POL-HT). In the final group, specimens were heat-treated according to 'polish and fire' cycle prior to manual polishing (HT-POL). To account for any variability induced by the ceramic blocks, cutting sequence or different individual firings, ten additional disk-shaped specimens were sequentially cut from a single prefabricated block and randomised. Subsequently, five specimens were manually polished as previously described (POL-HT_{SUPP}) before all ten disk-shaped specimens were heat treated according to 'polish and fire' cycle in a single furnace firing cycle. The remaining five samples were then polished (HT-POL_{SUPP}) after heat treatment.

2.3 Surface metrology

Surface metrology was conducted on each disk-shaped specimen to discriminate between differences in the surface roughness introduced by specimen manufacture and post-machining processes. A Nexview 5000 optical profilometer (Zygo, USA) with a 10× Mirau objective lens and 2.0 x magnification provided a resolution of 0.1 nm in the z-axis and was used to determine the mean Ra-value from a 0.36 × 0.27 mm measurement area arbitrarily chosen on each sample close to the specimen centre.

2.4 Bi-axial flexure strength (BFS) determination

An ElectroPuls E3000 universal testing apparatus (Instron, USA) was used for bi-axial flexure strength (BFS) testing of the disk-shaped specimens using a ball-on-ring configuration. Disks were coaxially positioned on an 8.8 mm diameter knife-edge ring support. For CAD and CAD-HT groups, the unmarked specimen surfaces were placed in contact with the ring support. For the POL, POL-HT and HT-POL groups, the polished specimen surfaces were placed in contact with the ring support. The disks were centrally loaded with a 7.9 mm diameter stainless steel ball indenter at a crosshead speed of 1

mm/min. BFS (MPa) was calculated using a Timoshenko and Woinowsky Krieger formula [21] (Equation 1):

$$BFS = \frac{P}{h^2} \cdot [(1+\upsilon) \cdot \left[0.485 \cdot \ln\left(\frac{a}{h}\right) + 0.52\right] + 0.48] \qquad \text{Equation 1}$$

where P was the load at fracture (N), ν the Poisson's ratio (0.22) [8], a the radius of the knife-edge support (mm) and h the mean thickness of the fracture surface (mm) measured with a screw-gauge micrometre with precision of 10 μm.

2.5 Scanning electron microscopy (SEM) and failure analysis

The fractured fragments from BFS testing were sputter coated with an Au/Pd coating and the fracture surfaces were imaged in a Hitachi S-4800 SEM (Hitachi High-Technologies, Japan) at 200 × magnification with an operating voltage of 5 kV. For each disk-group, specimens corresponding to low and medium (i.e. near average) BFS values were selected for imaging and analysed qualitatively to locate fracture origins. Additionally, SEM was employed to identify the nature of any surface and/or subsurface damage associated with the specimen fabrication process.

2.6 X-ray diffraction (XRD) analysis

XRD was performed to identify changes in crystalline content following the heat treatment protocol used in the study. X-ray diffraction patterns were collected with a Rigaku Ultima IV diffractometer (Rigaku Corporation, Japan) using a Cu-source (λ = 1.54 Å, 40 kV, 44 mA). The scans were recorded in the 2θ range from 15-40° with a 0.05° step interval and scan speed of 2°/min. Measurements were acquired for polished (POL) and polished heat-treated (POL-HT) surfaces.

2.7 Surface hardness and effect of heat treatment on controlled defects.

To identify whether heat treatment resulted in a change in surface hardness, Vickers hardness measurements (1 Kgf /10 s) were performed on polished (POL) and polished heat-treated (POL-HT) surfaces using a Wilson® Vickers Micro-hardness Tester (Buehler, USA) (n=15). In addition, to identify whether heat treatment could modify radial and lateral surface cracks, a series of Vickers

indents were generated on POL surfaces using different loads (0.5, 1 and 2 Kgf /10 s) and the radial crack lengths recorded (n=10 indents per load). Indented specimens (n=3) were subsequently heat treated and the radial crack lengths re-measured. Complementary characterization of ceramic surfaces using Atomic Force Microscopy (AFM) and SEM was carried out adjacent to the controlled indents before and after heat treatment to identify surface displacements which may potentially be associated with modification of lateral cracks and or the plastically deformed Vickers indentation zone. AFM was performed using a Dimension Edge AFM (Bruker, USA) using a monolithic silicon probe in tapping mode, a scan size of 30 × 30 μm and scan rate of 30 μm/s. SEM measurements were taken using a Zeiss EVO MA10 (Zeiss, Germany) on un-sputtered surfaces at numerous magnifications with an operating voltage of 5 kV.

2.8 Statistical analysis

A two-way analysis of variance (ANOVA) was used to determine differences between the mean BFS values of the disk-groups (CAD, CAD-HT, POL and POL-HT). The dependent variables were fabrication route (CAD-CAM vs sectioning/polishing) and post-machining heat treatment (none vs applied). A further one-way ANOVA and post-hoc Tukey tests were used to determine differences in the mean BFS values of the disk-groups (CUT, POL, POL-HT and HT-POL). An equivalent statistical approach was used to determine differences in surface roughness (mean Ra-values). An independent t-test was used to compare surface hardness before and after heat treatment and paired t-tests were used to identify whether Vicker's indent associated radial crack lengths were modified by heat treatment regime employed. All statistical tests were applied with significance level of $\alpha = 0.05$.

3. Results

3.1 Bi-axial flexure strength (BFS) determination

The two-way ANOVA identified that mean BFS value was significantly dependent on specimen fabrication route ($p<0.01$) and post-machining heat treatment ($p=0.04$). However, a significant factorial interaction ($p<0.01$) indicated that the magnitude of change in mean BFS value following heat treatment was dependent on fabrication route which determined the initial surface condition. The POL group specimens fabricated by sectioning and surface polishing exhibited a significantly higher ($p<0.01$) mean BFS (290 ± 86 MPa) when compared with the CAD group (137 ± 8.7 MPa). Heat treatment of the machined specimens (CAD-HT) resulted in a significant strengthening over the CAD group to 220 ± 16 MPa ($p<0.01$), whereas heat treatment of the sectioned and polished specimens (POL-HT) resulted in no significant change ($p=0.114$)) in mean BFS at 270 ± 50 MPa compared to CUT or POL groups **(Figure 1)**.

The mean BFS of the three groups of samples exhibiting a polished surface finish was significantly different ($p<0.01$) despite no significant difference in the mean surface roughness **(Table 1)**. However, significant strengthening relative to the as-cut surface condition (CUT) was only achieved by polishing specimens after heat treating (HT-POL) where the mean BFS was increased by ~50% ($p<0.01$). For the POL and POL-HT groups no significant strengthening was achieved relative to the CUT condition despite significant changes to the mean surface roughness introduced by the applied post-machining processes **(Table 1)**.

To further study initial results, ten additional disk-shaped specimens fabricated from the same substrate block were heat treated simultaneously. Five disk-shaped specimens were polished before (POL-HT_{SUPP}) and five disk-shaped specimens were polished after heat treatment (HT-POL_{SUPP}). No significant differences were identified between mean BFS values for POL-HT and POL-HT_{SUPP} ($p>0.05$) or between HT-POL and HT-POL_{SUPP} ($p>0.05$), thereby confirming the original findings (**Table 1**). CAD-CAM manufacture resulted in significantly higher mean surface roughness values compared with the polished samples. Heat treatment made no statistically significant difference to the

mean Ra-value for either surface condition ($p>0.05$). Similarly heat treatment made no significant difference to the Vicker's hardness of the polished surfaces ($p>0.05$), irrespective of whether polishing preceded or followed heat treatment (**Table 1**).

3.2 X-ray diffraction (XRD) analysis

XRD identified lithium metasilicate, lithium disilicate and lithium orthophosphate phases which were unaltered following heat treatment (**Figure 2)**. SEM images of the fracture surfaces revealed widespread submicron sized porosity within the machined ceramic microstructure which appeared to be reduced following heat treatment (**Figure 3**). Many of the disk-shaped specimens showed evidence of machining introduced damage in the form of median and radial cracks at sites either coincident with or peripheral to the failure origin. This was not limited to the CAD-CAM manufactured specimens with similar features also observed in low strength polished samples (**Figure 3**).

3.3 Surface hardness and effect of heat treatment on controlled defects

The impact of heat treatment on controlled surface defects (Vicker's indents with associated radial cracks) was observed using optical microscopy, SEM and AFM. Radial cracks <125 μm in length showed a tendency to reduce in length following heat treatment, whereas larger cracks >150 μm were either increased or decreased in length (**Figure 4**). A SEM image of a Vicker's indent which was associated with a decrease in radial crack length following heat treatment is shown in **Figure 5**. In addition to the crack length reduction, there was a rounding of the central plastically deformed indentation zone and a loss of sharp surface features. At lower magnification, a reduction in surface porosity in the polished surface containing the controlled indents was also evident. AFM measurements of regions of surfaces adjacent to Vicker's indents confirmed crack closure following heat treatment in some cases. However, in other cases, vertical displacement of the surface on one side of a radial crack was evident and was attributed to the extension of subsurface lateral cracks **(Figure 6)**.

4. Discussion

While a CAD-CAM production route offers the expedited delivery of indirect dental prosthesis, it also presents inherent challenges for the management of defects generated in ceramic surfaces during the manufacturing process. For ceramics machined in the fully crystallized state, the post-machining processes available to mitigate surface damage are practically limited to heat treatments at the annealing temperatures. Accordingly, there is a need to optimise the 'as machined' surface condition to prevent early clinical failures. Two subtractive machining processes, namely clinically representative CAD-CAM and sectioning using a slow speed diamond saw, to produce disk-shaped specimens were employed in the current study to generate test specimens of equivalent nominal dimensions. In general, material removal relied on the generation of concentrated contact stresses between the abrasive particles embedded in the machining tools and the ceramic surface leading to microfractures and chip generation [15-17]. However, the parameters known to influence surface damage accumulation including material removal rate, contact forces, localised heating and plastic deformation [15-17,22] differed for both approaches. The impact of the machining parameters on resultant mean BFS values were evident with the CAD Celtra® Duo specimens exhibiting only 50% of the mean BFS values of the CUT group. Differences in the superficial surface condition were detected using surface profilometry with the CAD-CAM surface exhibiting a four-fold higher mean Ra-value compared with the CUT group. However, subtractive machining of ceramics using multi-point contact grinding generates surface and subsurface damage in the form of median and lateral crack systems [23,24] which do not necessarily correlate with the microscopic surface roughness [1]. In addition, cracks in the CAD-CAM surface can be further stabilised or destabilised by zones of plastic deformation generated during machining [2,16]. Polishing of the as-cut specimen to generate the POL group resulted in the removal of ~20 μm of material from the disk-surface and resulted in a 50% reduction in the mean Ra-value, with no concomitant improvement in the mean BFS values. In **Figure 1** it is evident that polishing resulted in a considerable strengthening for a small number of specimens while for others there were noticeable strength reductions. Polishing reduces the length of cracks perpendicular to the surface that were originally generated during sectioning, and therefore an increase in mean BFS value would have been expected.

The lack of a strength increase can be explained by the fact that the surface removed is known to contribute to a compressive residual stress state, thereby stabilising these same defects [3,17]. The subsequent polishing may act to cause crack extension of the lateral crack systems which then have a greater contribution to the specimen failures. Evidence of lateral cracks close to the polished surface and associated with the fractographic failure origin are clearly distinguishable in the electron micrographs of the fracture surfaces in **Figure 2**.

Despite being advocated for clinical use in an the as-machined state, the manufacturer acknowledged that Celtra® Duo was strengthened following a short thermal treatment which can be simultaneously used for glazing and staining [13]. In contrast to a recent report [25], XRD measurements identified limited changes to the crystalline structure associated with heat treatment, which was consistent with most evidence for these systems [10-12]. During heat treatment, the peak temperature reached 820°C exceeding the glass softening temperature of the material which was reported at ~800°C [13]. In this state, the ceramic was a highly viscous liquid capable of limited flow which was seen here to result in a reduction of internal (**Figure 2**) and surface micro-porosity (**Figure 5**).

In the current study, the impact of heat treatment on BFS was significantly dependent on the fabrication route and initial surface condition. For the clinically relevant CAD-CAM specimens, heat treatment resulted in a significant strengthening which was not observed for the POL group. An assumption that the CAD-CAM surface was associated with initially larger critical defects than the POL surface can be made from the BFS data. The effect of the heat treatment on controlled surface defects introduced by Vicker's indentation was shown in **Figure 4** and highlighted that crack length reduction was sensitive to the initial crack dimensions. Surface damage associated with abrasive machining of ceramics has frequently been considered as a population of indentation sites which interact with each other and approximate for both the crack populations and the plastic deformation. It is acknowledged that while the Vicker's indent defect may not be identical to that generated by a clinical CAD-CAM route, it can be taken as a reasonable approximation in this case to systematically study defect behaviour in response

to heat treatment processes. In this study, radial cracks <125 μm in length reduced in dimension following heat treatment with the greatest reduction evident for initial crack lengths of 100-125 μm. Crack length reduction can be visualised in **Figure 5** which also highlighted that the plastically deformed zone at the indentation site, which exerted residual stresses on adjacent crack systems, was modified by the heat treatment. AFM measurements shown in **Figure 6** revealed that for some of the features that showed no crack length reduction following heat treatment, there was out-of-plane crack surface displacements. While not explicitly investigated in this study, it is postulated here that the out-of-plane crack displacement may result from differential cooling across larger crack surfaces including in lateral sub-surface defects. It was also noted that a deleterious mismatch in the coefficient of thermal expansion between the crystalline and glassy phases of Celtra® Duo has previously been reported which may have further contributed to the observed behaviour [26]. These outcomes have illustrated that while post-machining heat treatment may indeed mitigate the majority of defects inherently generated through the CAD-CAM route, the potential exists for geometries of defects where heat treatment may not reduce severity.

The most unexpected finding of the study related to the order of procedures applied for the polished disk-shaped specimen surfaces. Delaying surface polishing until after heat treatment resulted in a mean BFS value of 410 ± 77 MPa compared with 270 ± 50 MPa for specimens polished prior to heat treatment. The findings were subsequently confirmed by additional experiments to account for potential confounding factors, and the data are shown in **Table 1**. The POL-HT and HT-POLspecimens exhibited equivalent surface roughness (Ra-values), microstructure and surface hardness at the time of strength determination. The clinical relevance of the data is questionable given that the fit surface would not be polished prior to resin-cementation. However, the findings highlighted that it cannot be assumed that pre-cementation procedures that have the potential to modify the as-fabricated surface condition will have an equal impact irrespective of the timing of application relative to the applied heat treatment. In this study it has been demonstrated that the mechanical behaviour of a single CAD-CAM ceramic material is not only highly sensitive to the manufacturer's 'optional' heat treatment, but it is also

sensitive to the order of the procedures that are conceivable in clinical usage. The simplified circular disk geometry and ball-on-ring BFS testing was utilized for its approximation of the biaxial stress state that may occur at the fit surface of a restoration, though it is understood that more complex geometry and loading scenarios, namely dynamic loading, which routinely occur in vivo may influence the reported results.

5. Conclusions

The presented work demonstrated that the order of post-manufacture heat treatment and polishing operations influenced the mechanical performance when using a fully crystallized lithium silicate substrate. Beyond showing that the CAD-CAM production route decreases the mechanical performance compared with idealized surfaces, it was also demonstrated that the respective defect response to heat treatment differed markedly. There is a risk that digital pathways may create an overconfidence amongst practitioners in the predictability of CAD-CAM materials when compared with traditionally established processing routes, particularly for CAD-CAM materials where strength is statistically determined by defects introduced at the time of manufacture.

Future work should focus on systematic damage mitigating techniques to improve the mechanical performance of CAD-CAM production routes that would allow for the tight and repeatable tolerancing required when used clinically.

Acknowledgements

N.S. and S.V. were funded in part through BioTalent Canada Student Workplace Program. The authors would also like to acknowledge financial support through the University of Alberta Fund for Dentistry, the Department of Mechanical Engineering (University of Alberta), and the Natural Sciences and

Engineering Research Council of Canada. The authors would like to acknowledge Dr Ysidora Torrealba Martinez (University of Alberta) for her assistance with sample preparation.

References

1. Romanyk DL, Martinez YT, Veldhuis S, Rae N, Guo Y, Sirovica S, Fleming GJP, Addison O. Strength-limiting damage in lithium silicate glass-ceramics associated with CAD-CAM. Dent Mater 2019;35:98-104.

2. Rice RW, Mecholsky JJ. The nature of strength controlling machining flaws in ceramics. NBS Special Publication: The Science of Ceramic Machining and Surface Finishing II. US Government Printing Office, Washington DC;1979

3. Le DT. Optimization of machining performance of dental ceramic restorative materials. MS 97-1. University of Maryland, Maryland;1997

4. Malkin S, Ritter JE. Grinding mechanisms and strength degradation for ceramics. ASME J End Ind 1989;111:167-174.

5. Guess PC, Schultheis S, Bonfante EA, Coelho PG, Ferencz JL, Silva NR. All-ceramic systems: laboratory and clinical performance. Dent Clin North Am 2011;55:333-352.

6. Rauch A, Reich S, Dalchau L, Schierz O. Clinical survival of chair-side generated monolithic lithium disilicate crowns:10-year results. Clin Oral Investig 2018;22:1763-1769.

7. Pieger S, Salman A, Bidra AS. Clinical outcomes of lithium disilicate single crowns and partial fixed dental prostheses: a systematic review. J Prosthet Dent 2014;112:22-30.

8. Belli R, Wendler M, de Ligny D, Cicconi MR, Petschelt A, Peterlik H, et al. Chairside CAD/CAM materials. Part 1: Measurement of elastic constants and microstructural characterization Dent Mater 2017;33:84-98.

9. Wendler M, Belli R, Petschelt A, Mevec D, Harrer W, Lube T, Danzer R, Lohbauer U. Chairside CAD/CAM materials. Part 2: Flexural strength testing. Dent Mater 2017;33:99-109.

10. Apel E, van't Hoen C, Rheinberger V, Holand W. Influence of ZrO2 on the Crystallization and Properties of Lithium Disilicate Glass-Ceramics Derived from a Multi-Component System. J Eur Ceram Soc 2007;27:1571-1577.

11. Lin CC, Shen P, Chang HM, Yang YJ. Composition dependent structure and elasticity of lithium silicate glasses: Effect of ZrO2 additive and the combination of alkali silicate glasses. J Eur Ceram Soc 2006;26:3613-3620.

12 Krüger S, Deubener J, Ritzberger C, Höland W. Nucleation kinetics of lithium metasilicate in ZrO2-bearing lithium disilicate glasses for dental application. Int J Appl Glass Sci 2013;4:9-19.

13. Celtra Duo, Developed to make a difference, brochure for the dental laboratory. 22284/REV2017-08, Dentsply Sirona. 2017.

14. Addison O, Cao X, Sunnar P, Fleming GJP. Machining variability impacts on the strength of a 'chair-side' CAD-CAM ceramic. Dent Mater 2012;28:880-887.

15. Marshall DB, Evans EG, Khuri Yakub BT, Tien JW, Kino GS. The nature of machining damage in brittle materials. Proc R Soc Lond. 1983;385:461-475.

16. Zhang GM, Satish KG, Ko WK. The mechanics of material removal mechanisms in machining ceramics. Technical report TR 94-22rl. Institute for Systems Research (NIST), Maryland; 1994.

17. Hu KX, Chandra A. A fracture mechanics approach to modelling strength degradation in ceramic grinding processes. J Eng Ind 1993;115:73-83.

18. Rekow D, Thompson VP. Near-surface damage - A persistent problem in crowns obtained by computer-aided design and manufacturing. Proc Inst Mech Eng H 2005;219:233-243.

19. Sindel J, Petschelt A, Grellner F, Dierken C, Greil P. Evaluation of subsurface damage in CAD/CAM machined dental ceramics. J Mater Sci Mater Med. 1998;9:291-295.

20. Denry IL, Holloway JA, Tarr LA. Effect of heat treatment on microcrack healing behaviour of a machinable dental ceramic. J Biomed Mater Res 1999;48:791-796.

21. Timoshenko S, Woinowsky-Krieger S. Symmetrical bending of circular plates. In: Theory of plates and shells. 2nd ed. New York: McGraw-Hill; 1959.

22. Chen XP, Xiang ZX, Song XF, Yin L. Machinability: Zirconia-reinforced lithium silicate glass ceramic versus lithium disilicate glass ceramic. J Mech Behav Biomed Mater 2020;101:1034352.

23. Rice RW, Mecholsky JJ, Becher PF. The effect of grinding direction on flaw character and strength of single and polycrystalline ceramics. J Mater Sci 1981;16:853-862.

24. Conway JC, Kirchner HP. The mechanics of crack initiation and propagation beneath a moving sharp indenter. J Mater Sci 1980;15:2879-2883.

25. Riquieri H, Monteiro JB, Viegas DC, Campos TMB, de Melo RM, de Siqueira Ferreira Anzaloni Saavedra G. Impact of crystallization firing process on the microstructure and flexural strength of zirconia-reinforced lithium silicate glass-ceramics. Dent Mater 2018;34:1483-1491.

26. Wendler M, Belli R, Lohbauer U. Factors influencing development of residual stresses during crystallization firing in a novel lithium silicate glass-ceramic. Dent Mater 2019;35:871-882.

Table 1: The mean biaxial flexure strength values, mean surface roughness (Ra-values) and Vickers Hardness Numbers (mean +/- SD) for disk-groups where the dependent variables were fabrication route and post-machining heat treatment . One-way ANOVAs and post-hoc Tukey tests were employed to determine differences in the mean BFS values and surface roughness. An independent t-test was used to compare Vickers Hardness Number. All statistical tests were applied with significance level of α = 0.05 and different subscript denominations between columns denoting significant differences (n=15).

	CAD	CAD-HT	CUT	POL	POL-HT	HT-POL
Biaxial Flexural Strength (MPa) (SUPP)	**137 ± 9** ^{a}	**220 ± 16** ^{b}	**280 ± 38** $^{b\,c}$	**290 ± 86** ^{c}	**270 ± 50** ^{c} (298 ± 66)^{c}	**410 ± 77** ^{d} (415 ± 71)^{d}
Surface Roughness Mean Ra-value (µm)	**4.5 ± 0.6** *	**4.6 ± 0.8** *	**1.1 ± 0.3** $^{\wedge}$	**0.5 ± 0.1** $^{\#}$	**0.5 ± 0.2** $^{\#}$	**0.6 ± 0.2** $^{\#}$
Vickers Hardness Number (HVN)	*	*	*	**672 ± 26**	**682 ± 37**	**708 ± 61**

Figure 1: Scatter plots summarizing the BFS data for Celtra® Duo disk-groups where the dependent variables were fabrication route and post-machining heat treatment . All data are shown (n=15 for each specimen group) with the mean BFS values and associated error bars which represent one standard deviation. Closed symbols represent groups which did not receive post-machining heat treatment while open symbols indicate groups of samples that have received heat treatment prior to BFS testing.

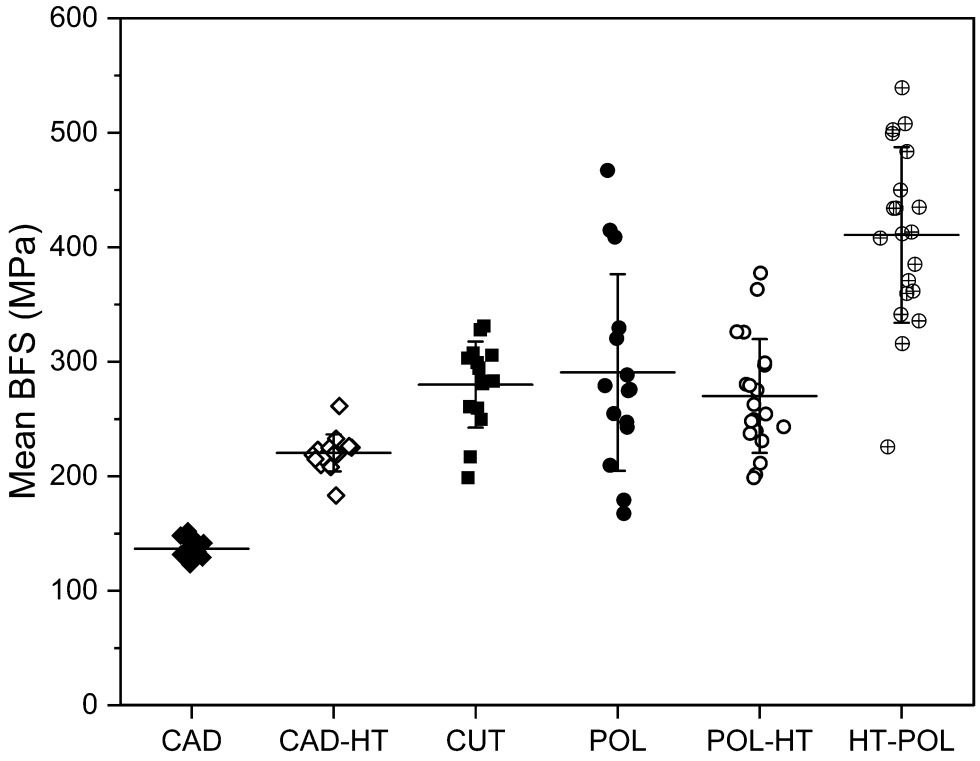

Figure 2: Scanning electron micrographs of (A) the as machined ceramic microstructure and (B) the post-machining heat treatment microstructure. Scanning electron micrographs of the fracture surfaces of (C) a CAD-CAM fabricated specimen (CAD), (D) a CAD-CAM heat-treated specimen (CAD-HT), (E) a polished specimen (POL) and (F) a polished and heat-treated specimen (POL-HT) for comparison and analysis. Red arrows highlight regions of lateral sub-surface cracks propagating from the fracture origin in CAD-CAM samples.

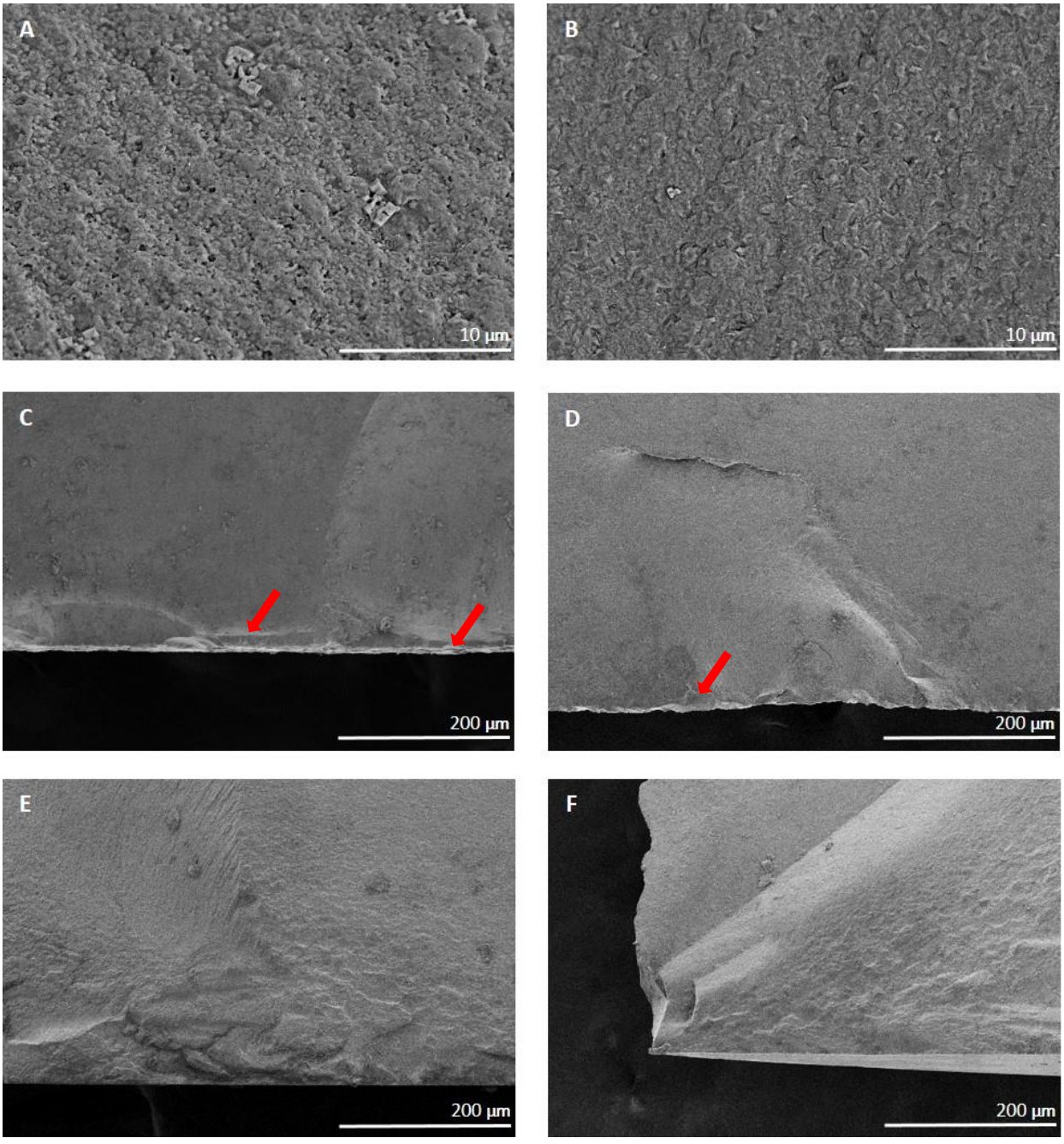

Figure 4: Scatter plot highlighting the relationship between the measured baseline radial crack length associated with a Vickers indentation introduced onto a polished surface (POL) and measured radial crack length following heat treatment (POL-HT). Three indentation forces (0.5, 1.0 and 2.0 Kgf) were used to create three discrete clusters of varying crack lengths. Significance values of the associated changes in radial crack length observed following heat treatment for each indentation force cluster are indicated with the associated Pearson correlation co-efficient (r).

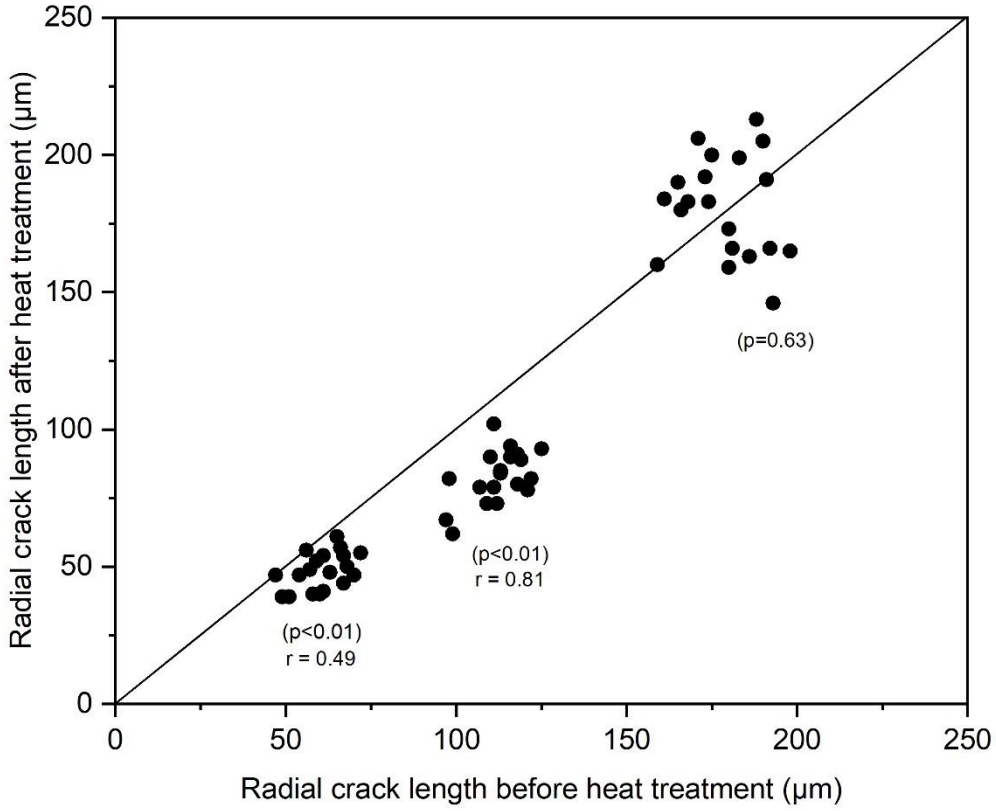

Figure 5: Scanning electron micrographs of the same region of a polished Celtra® Duo surface (POL) containing a series of Vickers indentations (A) before and (B) following heat treatment (POL-HT). The POL surface (A) demonstrates visible surface porosity which is considerably reduced following heat treatment (B). Scanning electron micrographs (C) and (D), respectively illustrate the introduction of a single Vickers indentation (1 Kgf, 10 s) introduced into the polished ceramic surface and the (C) baseline radial crack length associated with the indentation was measured before (POL) and (D) the measured radial crack length following heat treatment (POL-HT). Image quality of the selected scanning electron micrographs has been compromised somewhat by surfaced charging but conductive surface coating was not performed to avoid the introduction of a new variable between measurements following heat treatment. The surface indent in the polished surface (POL) is representative of sample repeats and shows an irregular plastically deformed compression zone, with damage extending beyond periphery of the indent site and two orthogonal radial cracks. Surface scratches associated with polishing with a final P2000 SiC abrasive paper dominate the background and allow for image superimposition. Following heat treatment (POL-HT), the indentation zone exhibits more rounded contours and the measured radial crack lengths are significantly reduced.

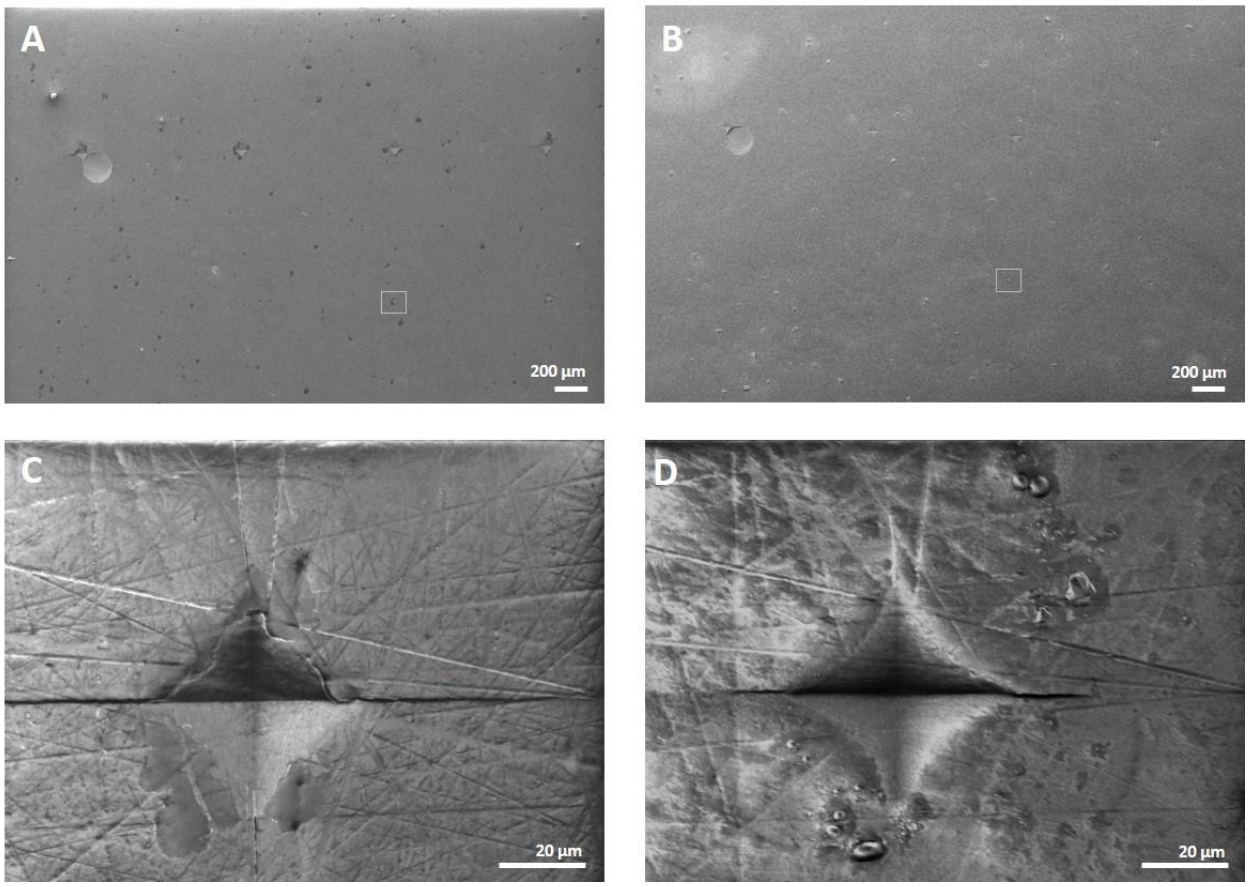

Figure 6: Atomic Force Microscopy (AFM) images of a polished Celtra® Duo surface (POL) adjacent to a Vickers indentation (2 Kgf, 10 s) introduced into the polished ceramic surfaces (A) before and (B) following heat treatment (POL-HT). Polishing features have been marked (*) on the two-dimensional images to aid image correlation. Both panels A and B include the region of a radial crack close to the plastically deformed indentation site and bisecting the surface polishing marks. In Panel A, following heat treatment, the surface polishing features remain, however, there has been an upward displacement of the surface adjacent on one side of the crack, likely due to the extension of subsurface lateral cracks introduced during the Vickers indentation process. In Panel B, the radial crack is observed to close with the crack walls becoming more tightly opposed and no associated upward deflection of the surface evident.